earthquakes 30 km deep (Fig. 1), and from the presence of incrementally raised shorelines (Table 1). Both the earthquakes and stranded shorelines occur near the former edges of the ice sheet.

Although only minor raised shorelines have been reported in Hudson Bay[24], Baffin Island seems to have eight on its western coast and nine on its eastern coast[18] (Table 1). On both coasts the stranded shorelines can be correlated over distances of 70 km, have vertical separations of ~13 m, and were created between 2,000 and 9,000 years ago. Uplifted shorelines are also found in southern Newfoundland, where as many as five strands separated by an average of 12 m can be found at one location[19]. In this case, the strands can be correlated over tens of kilometres, but they have not been accurately dated. The erosion surfaces behind all these shorelines are not grossly tilted (a maximum of 1 m km^{-1}), suggesting that they were raised in a block-like fashion by elastic rebound instead of on a doming isostatic adjustment.

The raised shorelines lie along the edges of eastern Canada's most seismically active zone, a mostly offshore belt running from the Great Lakes to Newfoundland and Baffin Island. This belt includes the 1929 Grandbanks $M = 7.2$ earthquake on the seaward-sloping continental shelf off Newfoundland, an event that produced a tsunami that killed 27 people and cut the first transatlantic telephone cable. As Fig. 1 shows, the belt includes zones where there is roughly a 1% chance per decade of horizontal accelerations exceeding 0.3 *g* (ref. 15). As in 1929, such rapid movements are enough to level unreinforced buildings.

Both the raised shorelines and seismicity are consistent with our ice-loading strain model. First, the loading and unloading of the crust seems to produce roughly the same number of events: six Heinrich events and seven or eight shoreline uplifts. Second, the strain rates and recurrence intervals scale with each other: the crust was unloaded one-and-a-half orders of magnitude faster than it was loaded. The resulting earthquake recurrence times would also be much shorter, on the order of 10^2–10^3 yr. Further, the intervals between the shoreline events increases with time (Table 1).

Studies of ice dynamics have led to the suggestion that the large volume of sediments associated with Heinrich events can be accounted for by a 'binge–purge' cycle in the ice cap[12]. This cycle begins with ice-sheet thickening, with consequent sub-ice melting and higher seaward flow rates, which in turn produces ice-sheet thinning, slowing down and attachment of saturated subglacial regolith by freezing. The binge is estimated to take ~8 kyr and the purge ~750 yr. This mechanism has been shown to be compatible with the Heinrich event sediment volumes, but it predicts that the event intervals would be uniform and sedimentation rates slow enough to include foraminifera. Our model can account for the rapid purge by nearly instantaneous shaking and failure of the edge of the ice load—in effect, the earthquakes removed the resisting toes of the glacial ice slides. The inherent spatial variability of earthquake epicentres is also consistent with the differences in the Heinrich layer sediments and ice sources.

In addition to searching for and dating the faults implied by our model for the Heinrich events, it can also be tested by studies of sedimentary structures, relations and ages near their origins. If, for example, undisturbed Heinrich layers immediately overlie slumped or otherwise seismic disturbed sediments, our case would be stronger. Such features might be recognized and mapped with reflection profiling. The model could also be strengthened by further dating and palaeoseismic studies of the raised shorelines, as well as a complete three-dimensional numerical simulation of the coupled ice dynamics and ice-load-induced failures.

We conclude by suggesting that if it is true that the Heinrich events were driven primarily by crustal, as opposed to orbital, mechanics, then so were their associated climate variations. It may be found that some ice-age climatic variations were feedback effects produced by earthquake-related unloading of the ice sheet. Such a finding would lead to a much simplified interpretation of the timescales of ice-age climate changes. □

Received 8 May 1997; accepted 16 March 1998.

1. Heinrich, H. Origin and consequences of cyclic ice rafting in the Northeast Atlantic Ocean during the past 130,000 years. *Quat. Res.* **29,** 142–152 (1988).
2. Andrews, J. T. & Tedesco, K. Detrital carbonate-rich sediments, northwestern Labrador Sea; implications for ice-sheet dynamics and iceberg rafting (Heinrich) events in the North Atlantic, *Geology* **20,** 1087–1090 (1994).
3. Bond, G. *et al.* Evidence for massive discharges of icebergs into the north Atlantic ocean during the last glacial period. *Nature* **360,** 245–249 (1992).
4. Grimm, E. C., Jacobson, G. L. Jr., Watts, W. A., Hansen, B. C. S. & Maasch, K. A. A 50,000 year record of climate oscillations from Florida and its temporal correlation with the Heinrich events. *Science* **261,** 198–200 (1993).
5. Lowell, T. V. *et al.* Interhemispheric correlation of late Pleistocene glacial events. *Science* **269,** 1541–1549 (1995).
6. Broecker, W. S. Massive iceberg discharges as triggers for global climate change. *Nature* **372,** 431–424 (1994).
7. Bond, G. *et al.* Correlations between climate records from North Atlantic sediments and Greenland ice. *Nature* **365,** 143–147 (1993).
8. Baltuck, M., Dickey, J., Dixon, T. & Harrison, C. G. A. New approaches raise questions about future sea level changes. *Eos* **77,** 385–388 (1996).
9. Shackleton, N. J., Imbrie, J. & Hall, M. A. Oxygen and carbon isotope record of East Pacific Core V19–30; implications for the formation of deep water in the late Pleistocene North Atlantic. *Earth Planet. Sci. Lett.* **65,** 233–244 (1983).
10. Bond, G. & Lotti, R. Climate forcing of millennial-scale ice rafting cycles in the North Atlantic. *Eos* **75,** 332 (1994).
11. Hays, J. D., Imbrie, J. & Shackleton, N. J. Variations in the earth's orbit: pacemaker of the ice ages. *Science* **194,** 11221–1132 (1976).
12. Alley, R. B. & MacAyeal, D. R. Ice-rafted debris associated with binge–purge oscillations of the Laurentide ice sheet. *Paleoceanography* **9,** 503–511 (1994).
13. Gupta, H. K. & Chandha, R. K. (eds) *Induced Seismicity* (*Pure Appl. Geophys.* Vol. 145**, 1995).**
14. Hasegawa, H. S. & Basham, P. W. in *Earthquakes at North-Atlantic Passive Margins: Neotectonics and Postglacial Rebound* (ed. Gregersen, S. and Basham, P. W.) 483–500 (NATO Advanced Study Institutes Series C, Vol. 266, 1989).
15. Geological Survey Canada, http://www.seismo.nrcan.gc.ca/sheishaz4gen123.html
16. Arvidsson, R. Fennoscandian earthquakes: whole crustal rupturing related to postglacial rebound. *Science* **274,** 744–745 (1996).
17. Johnston, A. C. A wave in the earth. *Science* **274,** 735 (1996).
18. Andrews, J. T. *A Geomorphological Study of Post-Glacial Uplift with Particular Reference to Arctic Canada* (London Institute of British Geographers, London, 1970).
19. Tucker, C. M., Leckie, D. A. & McCann, S. B. Raised shoreline phenomena and postglacial emergence in south-central Newfoundland. *Geomorph. Phys. Quat.* **36,** 165–174 (1982).
20. Lay, T. & Wallace, T. C. *Modern Global Seismology* (Academic, New York, 1995).
21. Broecker, W. *The Glacial World According to Wally* (Lamont-Doherty Earth Observatory, Palisades, 1995).
22. Cathles, L. M. III *The Viscosity of the Earth's Mantle* (Princeton Univ. Press, 1975).
23. Sieh, K. E. in *Earthquake Prediction* (ed. Simpson, D. W. and Richards, P. G.) 181–207 (American Geophysical Union, Washington, 1981).
24. Bird, J. B. *The Physiography of Arctic Canada* (Johns Hopkins Univ. Press, 1967).

Acknowledgements. We thank G. Bond and J. Park for insightful and considered reviews, and our colleagues for their patient help in understanding Heinrich events.

Correspondence and requests for materials should be addressed to P.E.M. (e-mail: pem@vaino.geo.duke.edu).

Sphenoid shortening and the evolution of modern human cranial shape

Daniel E. Lieberman

Department of Anthropology, Rutgers University, New Brunswick, New Jersey 08903-0270, USA

Crania of 'anatomically modern' *Homo sapiens* from the Holocene and Upper Pleistocene epochs differ from those of other *Homo* taxa, including Neanderthals, by only a few features. These include a globular braincase, a vertical forehead, a dimunitive browridge, a canine fossa and a pronounced chin[1–4]. Humans are also unique among mammals in lacking facial projection: the face of the adult *H. sapiens* lies almost entirely beneath the anterior cranial fossa, whereas the face in all other adult mammals, including Neanderthals, projects to some extent in front of the braincase. Here I use radiographs and computed tomography to show that many of these unique human features stem partly from a single, ontogenetically early reduction in the length of the sphenoid, the central bone of the cranial base from which the face grows forward. Sphenoid reduction, through its effects on facial projection and cranial shape, may account for the appar-

Table 1 Partial correlation matrix from cross-sectional samples of *Pan troglodytes* (top) and *Homo sapiens* (bottom)

	MFP	ACL	ASL	MFL	MCL	ECV
MFP	–	–0.292*	0.202*	0.728*	–0.124*	–0.009
ACL	–0.192*	–	0.460*	0.604*	–0.179*	0.158*
ASL	0.490*	0.211*	–	–0.424*	0.593*	–0.290*
MFL	0.663*	0.218*	–0.605*	–	0.572*	–0.316*
MCL	–0.166*	0.345*	0.572*	0.602*	–	0.753*
ECV	–0.110	–0.335*	–0.044*	–0.222	0.685*	–

*$P < 0.01$ (Fisher's *r*-to-*z*). Abbreviations. MFP, midfacial projection; ACL, anterior cranial base length; ASL, anterior sphenoid length; MFL, midfacial length; MCL, maximum cranial length; ECV, endocranial volume. See Methods for sample details and variable definitions.

ently rapid evolution of modern human cranial form, and suggests that Neanderthals and other archaic *Homo* should be excluded from *H. sapiens*.

Shortening of the sphenoid influences human cranial shape primarily by altering the spatial relationships between the face, cranial base and neurocranium in the sagittal plane, which together determine the degree of facial projection. Variations in facial projection (which is distinct from prognathism[5]) are a function of the relative anteroposterior growth of three developmentally distinct dimensions (Fig. 1a): anterior cranial base length (ACL); anterior sphenoid body length (ASL); and anteroposterior mid-facial length (MFL). ACL, between sella and the foramen caecum, elongates through bone deposition in basicranial synchondroses induced by brain growth. ASL increases as a result of forward expansion of the sphenoid body, and extends from sella to the posterior maxillary plane[6]. This plane, from the maxillary tuberosities to the junction between the middle and anterior cranial fossae, forms the boundary between the cranial base and the ethmo-maxillary complex that comprises most of the face[6–8]. Thus ASL determines the position of the back of the face relative to the cranial base. The final dimension that influences facial projection is MFL (see Fig. 1), the minimum distance from the posterior maxillary plane to nasion. The face elongates through sutural growth along its posterior margins and from appositional growth on its anterior surfaces[7]. Histological studies show, however, that the anterior aspect of the maxilla in humans, unlike non-human primates and australopithecines, is a resorptive field[9,10]. The human midface therefore elongates from deposition on its posterior surface, which displaces it forward relative to the posterior maxillary plane.

The contributions of ACL, ASL and MFL to facial projection were measured in recent and fossil *Homo* crania using lateral radiographs and computed tomography (CT) scans (see Methods). Longitudinal samples[11] indicate that these dimensions grow at different rates in *H. sapiens* (Fig. 2a). MFL elongates in a slow, skeletal growth trajectory, attaining 95% of adult length by 15–18 years, but ASL and ACL lengthen more rapidly, reaching 95% of adult size after approximately 4 and 6 years, respectively. The effects of these dimensions on facial projection were tested using partial correlation analyses of intraspecific, cross-sectional samples of humans and chimpanzees (Table 1). In these species, MFL, ACL and ASL make statistically significant and independent contributions to midfacial projection, independent of any effects of overall cranial size (maximum length and endocranial volume). MFL, ACL and ASL were all found to have

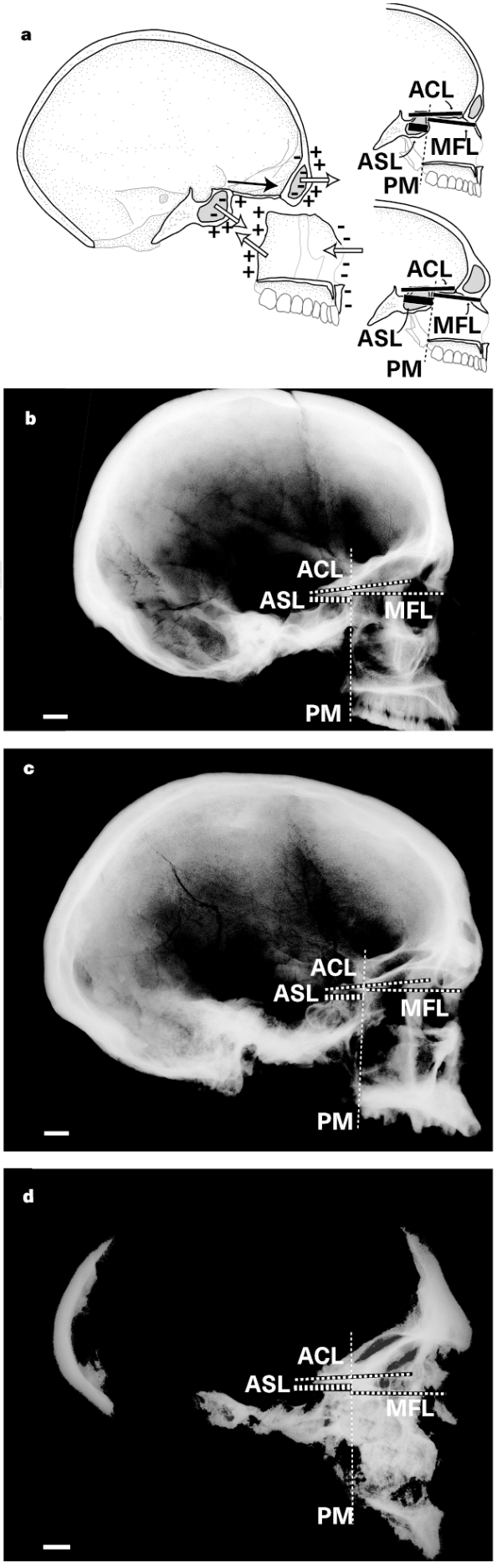

Figure 1 Cranial growth in modern and archaic *Homo*. **a**, Left, midsagittal diagram of anteroposterior growth processes in cranial base, braincase and face. Black arrows indicate synchrondrosal growth; white arrows indicate appositional growth (+) and resorption (–). Right, diagrams of *H. sapiens* (top) and Neanderthal (bottom) show the posterior maxillary (PM) plane, anterior cranial base length (ACL), midfacial length (MFL) and anterior sphenoid length (ASL) (see Methods). **b**–**d**, Lateral radiographs of: **b**, recent *H. sapiens* (Egyptian male); **c**, male Upper Pleistocene *H. sapiens* (Cro-Magnon I); **d**, female Neanderthal (Gibraltar I). ASL in the female Neanderthal is 20% longer than in the Upper Pleistocene male; ACL and MFL are approximately 15% shorter. Scale bars, 10 cm.

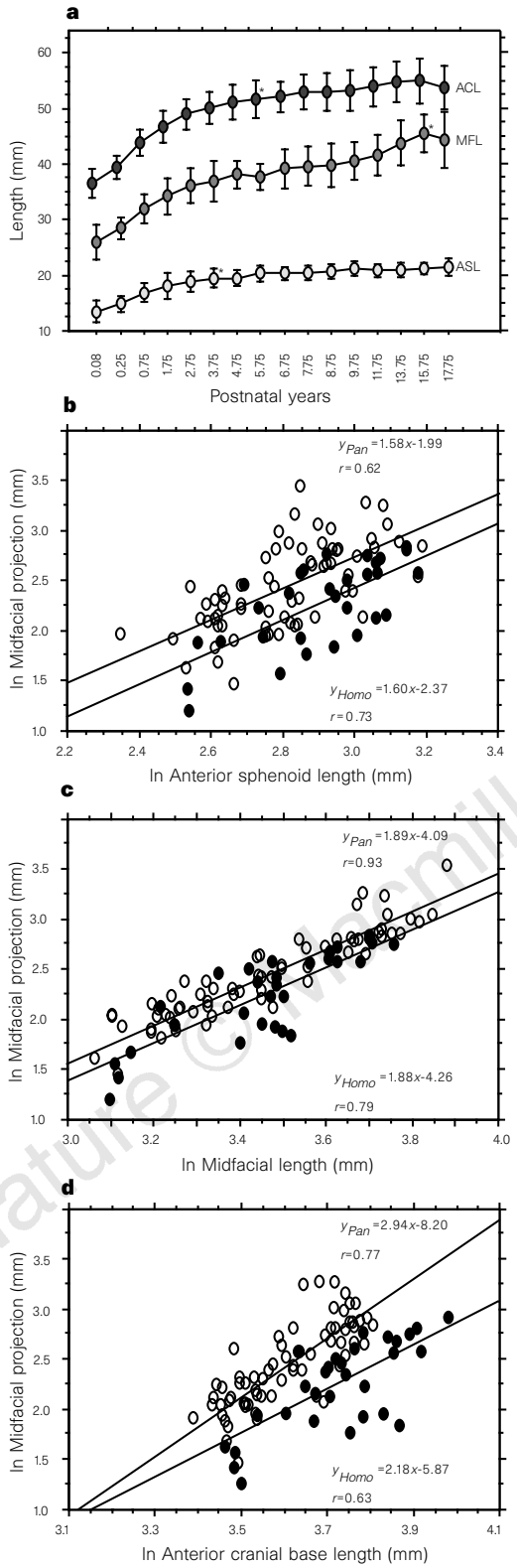

Figure 2 Ontogeny of facial projection in *Homo sapiens* and *Pan troglodytes*. **a**, Growth rates in longitudinal sample of *H. sapiens*[16] of anterior cranial base length (ACL), midfacial length (MFL) and anterior sphenoid length (ASL). Bars represent 1 standard deviation; asterisks indicate 95% of mean adult size. **b**–**d**, Log-transformed least-squares regression of these dimensions with midfacial projection in cross-sectional samples of *H. sapiens* (filled circles) and *P. troglodytes* (open circles). See Methods for measurement and sample details.

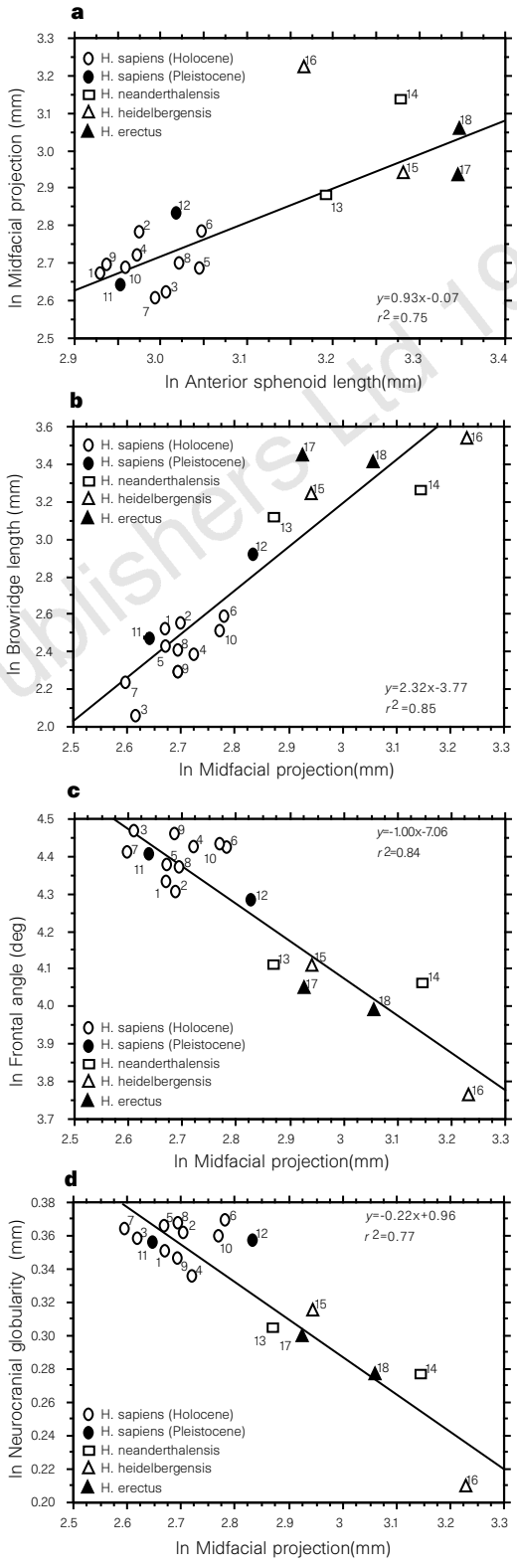

Figure 3 Effects of anterior sphenoid length (ASL) on facial projection (MFP) and other aspects of cranial shape in *Homo*. **a**, Log-transformed least-squares regression of ASL with MFP (including *H. heidelbergensis*, $y = 1.01x - 0.30$; $r^2 = 0.620$). **b**–**d**, Log-transformed least-squares regressions between MFP and supraorbital length, frontal angle and midsagittal cranial curvature (see Methods). Samples include: 1, female Australians; 2, male Australians; 3, female Chinese; 4, male Chinese; 5, female Italians; 6, male Italians; 7, female Egyptians; 8, male Egyptians; 9, female Ashanti; 10, male Ashanti; 11, female Pleistocene *H. sapiens*; 13, female Neanderthal; 14, male Neanderthals; 15, female *H. heidelbergensis*; 16, male *H. heidelbergensis*; 17, female *H. erectus*; and 18, male *H. erectus*.

Table 2 Intertaxon analysis of variance of facial, basicranial and neurocranial dimensions and spatial relationships in *Homo*.

Taxon	*N* (m/f)	ASL (mm)	ACL (mm)	MFL (mm)	LFL (mm)	MFP (mm)	FRA (mm)	SOL (mm)	GLO (mm)	MCL (mm)	ECV (cm^3)
H. sapiens (Holocene)	100 (50/50)	19.9 (2.0)	47.8 (2.9)	40.6 (3.6)	45.0 (3.8)	14.6 (2.4)	81.4 (6.4)	11.1 (2.7)	1.41 (0.1)	177.7 (8.2)	1,368.4 (149.4)
H. sapiens (Pleistocene)	6 (4/2)	20.0 (1.8)	49.6 (3.7)	45.4* (2.3)	50.8* (6.5)	16.1 (2.1)	77.5 (5.4)	17.0* (3.0)	1.43 (0.1)	193.0* (10.0)	1,478.8 (114.8)
H. neanderthalensis	5 (3/2)	25.9*† (2.9)	52.6* (7.1)	46.9* (4.9)	52.6* (7.5)	21.4*† (4.8)	59.0*† (6.0)	24.8*† (2.8)	1.33† (0.1)	198.3* (11.3)	1,447.5 (201.1)
H. heidelbergensis	3 (2/1)	24.8*† (5.1)	48.8 (9.1)	45.3* (8.5)	53.0* (9.5)	24.6*† (10.1)	49.0*† (10.8)	31.5*† (6.0)	1.32† (0.0)	200.3* (13.5)	1,201.7* (93.9)
H. erectus	2 (1/1)	28.4*† (0.1)	35.3* (1.6)	39.6 (3.4)	48.7	20.0*† (1.8)	55.5*† (2.1)	30.5*† (0.6)	1.34*† (0.0)	190.5* (20.5)	935.5*† (185.9)

See Methods for sample details and variable definitions. Standard deviations are in parentheses. Abbreviations: ASL, anterior sphenoid length; ACL, anterior cranial base length; MFL, midfacial length; LFL, lower facial length; MFP, midfacial projection; FRA, frontal angle; SOL, supraorbital length; GLO, neurocranial curvature (globularity); MCL, maximum cranial length; ECV, endocranial volume.
* Significantly different ($P < 0.01$, Scheffé's F) from Holocene *H. sapiens*.
† Significantly different ($P < 0.01$, Scheffé's F) form Pleistocene *H. sapiens*.

strong, positive allometric effects on facial projection (Fig. 2b–d). Variations in facial projection in chimpanzees, humans and presumably fossil hominids derive, therefore, from differences in MFL, ACL and ASL, all of which influence the position of the front of the face relative to the cranial base and neurocranium.

Although facial, cranial base and sphenoid length each affect facial projection in modern humans and other primates, comparisons between taxa show that variations in ASL provide the main structural basis for the differences in facial projection between Pleistocene 'anatomically modern' *H. sapiens* and archaic *Homo*. Midfacial length, lower facial length, anterior cranial base length and endocranial volume do not differ significantly between adult Pleistocene modern *H. sapiens*, Neanderthals and *H. heidelbergensis* (Table 2). In contrast, ASL is roughly 30% shorter ($P < 0.001$) in Holocene and Pleistocene modern *H. sapiens* than in Neanderthals and other archaic *Homo* taxa (Fig. 1b–d). Anterior sphenoid shortening reduces facial projection in crania of Pleistocene and Holocene *H. sapiens* compared with crania of archaic *Homo* by positioning the posterior maxillary plane, and hence the posterior margin of the face, closer to the middle cranial fossa. ASL accounts for approximately 75% of the variation in facial projection among Pleistocene fossil and Holocene taxa of the genus *Homo* (Fig. 3a; excluding *H. heidelbergensis* males, in which a significantly longer MFL than other archaic *Homo* taxa ($P < 0.05$) contributes to an extreme degree of facial projection).

Reduced facial projection in modern humans, which results primarily from sphenoid shortening, results in other phylogenetically and functionally significant differences in craniofacial shape. Facial projection is the main influence on browridge size and frontal angulation in non-human primates[12–14], and contributes to roughly 85% of the variation in these features in *Homo* (Fig. 3b, c). Reduced facial projection also increases overall cranial globularity in modern humans by decreasing cranial length relative to endocranial volume (Fig. 3d). Finally, decreased facial projection positions the maxilla closer to the foramen magnum and the temporo-mandibular joint in *H. sapiens* than in archaic *Homo*, reducing the length of the oropharynx and the load arm of the chewing muscles[15,16]. But sphenoid shortening is not the only source of variation in facial projection and its consequent effects in *Homo*. Within *Homo*, r^2 is 0.74 between ASL and browridge length, 0.65 between ASL and frontal angle, and 0.47 between ASL and cranial globularity. Within *H. sapiens*, for example, variations in facial projection result mostly from differences in MFL, which is approximately 12% shorter in Holocene than Pleistocene populations ($P < 0.01$), and from a similar decrease in overall cranial size (Table 2). These factors account for the considerable morphological variability in browridge size and other features in Pleistocene *H. sapiens* crania, such as that evident in the Skhul and Qafzeh hominids[17].

Given the close phylogenetic relationship between *H. sapiens*, Neanderthals and other Pleistocene hominid taxa, it should perhaps not be surprising that many unique features of the modern human cranium apparently result from a single, ontogenetically early, shift in cranial base growth. The discrete, derived developmental basis of sphenoid shortening in *H. sapiens*, together with its effects on craniofacial shape, may explain how modern humans might have evolved rapidly from more archaic forms, possibly as a distinct clade, and arguably as a distinct phylogenetic species[18–20]. Other aspects of cranial shape that distinguish recent and Pleistocene modern *H. sapiens* populations[4,21] probably result from decreases in facial length, brain size and overall skeletal robusticity[4,22,23]. The complex, integrated nature of craniofacial growth and function make it unlikely, however, that any single selective advantage can account for the evolution of sphenoid shortening and the unique craniofacial configuration of *H. sapiens*. One possibility is that a shorter sphenoid, by decreasing the oropharynx length, is an adaptation for speech. If the hyoid and larynx had the same low position relative to the mandible and cranial base in archaic *Homo* that they do in *H. sapiens*[24], a shorter sphenoid would contribute to the unique proportions of the human vocal tract, in which the horizontal component is roughly equal in length to its vertical component, rather than markedly longer as in other primates[25]. This configuration improves the ability to produce acoustically distinct speech sounds[25–27], and so may have provided some advantage for sphenoid reduction and its consequent effects on facial projection in *H. sapiens*. □

Methods

Samples used. Lateral radiographs were taken of 20 adult (10 males and 10 females) recent *H. sapiens* crania from Australia, south China, Europe (Italy), north Africa (Egypt), and sub-Saharan Africa (Ashanti) from the American Museum of Natural History (AMNH); a pooled-sex cross-sectional sample ($n = 30$) of modern human crania from the Cleveland Museum of Natural History (CMNH); and a longitudinal sample of 16 males and 16 females from the Denver Growth Study radiographed from 1 month to 18 years after birth[11]. A cross-sectional, pooled-sex sample ($n = 69$) of *Pan troglodytes* (chimpanzee) was radiographed from collections at the AMNH, the CMNH and the Museum of Comparative Zoology (Harvard). The cross-sectional human and chimpanzee samples include equal numbers of individuals from four dental stages (before eruption of the first upper molar (M^1); after M^1 eruption before M^2 eruption; after M^2 eruption but before M^3 eruption; and after M^3 eruption).

The fossil sample includes crania for which radiographs and/or CT scans are available and which are sufficiently complete to reconstruct the posterior maxillary plane and other aspects of facial position relative to the basicranium and neurocranium. The posterior maxillary plane maintains an angle of 90° with the neutral horizontal axis of the orbit throughout postnatal development in *H. sapiens* (angle $x = 89.9°$, s.d. $= 1.7$, $n = 353$) as it does in all mammals, including *P. troglodytes*[6,8]. This constant angle allows accurate reconstruction of the posterior maxillary plane in fossils well-preserved maxillary tuberosities and orbits. Fossils used were split by sex into the following groups: male early modern *H. sapiens* (Cro Magnon I, Obercassel I, Skhul IV and V); female early

modern *H. sapiens* (Abri Pataud, Obercassel II); male Neanderthals (La Chapelle aux Saints, La Ferrassie I, Monte Circeo, La Quina V); female Neanderthals (Gibraltar I); male *H. heidelbergensis* (Broken Hill, Petralona); female *H. heidelbergensis* (Steinheim); male *H. erectus* (OH 9); female *H. erectus* (KNMR-ER 3733). I radiographed all crania except for Skhul IV (B. Arensburg), Petrolona (C. Stringer), KNM-ER 3733 (A. Walker) and Obercassel I and II, Monte Circeo, La Quina V (T. Molleson). F. Spoor provided CT scans of the OH 9, Broken Hill and Steinheim specimens.

Measurements. Linear and angular measurements were taken from traced radiographs using digital calipers accurate to 0.01 mm, and a protractor accurate to 1°. Measurements include: ASL (anterior sphenoid body length), the minimum distance from the sella to the posterior maxillary plane; ACL (anterior cranial base length), from the sella to the foramen caecum; MFL (midfacial length), the minimum distance from the posterior maxillary plane to nasion; LFL (lower facial length), from the anterior nasal spine to the posterior nasal spine; MFP (midfacial projection) from nasion to the foramen caecum (perpendicular to the posterior maxillary plane); FRA (frontal angle) from the metopion to the base of the frontal squama relative to the Frankfurt horizontal; SOL (supraorbital length) from the glabella to fronton (perpendicular to the posterior maxillary plane); GLO (neurocranial curvature or globularity) from the glabella to the opistocranion; and ECV (endocranial volume), which was measured by filling crania with beads; estimates of fossil endocranial volume are from ref. 28. For landmark definitions, see ref. 29.

Received 6 October 1997; accepted 10 February 1998.

1. Day, M. H. & Stringer, C. B. in *L'*Homo erectus *et la Place de l'Homme de Tautavel parmi les Hominides Fossiles* Vol. 2 (ed. De Lumley, H.) 814–846 (Louis-Jean, Nice, 1982).
2. Lieberman, D. E. Testing hypotheses about recent human evolution from skulls: integrating morphology, function, development and phylogeny. *Curr. Anthropol.* **36,** 159–197 (1995).
3. Kidder, J. H., Jantz, R. L. & Smith, F. H. in *Continuity or Replacement: Controversies in* Homo sapiens *Evolution* (eds Bräuer, G. & Smith, F. H.) 157–177 (A.A. Balkema, Rotterdam, 1992).
4. Lahr, M. M. *The Evolution of Modern Human Cranial Diversity* (Cambridge Univ. Press, 1996).
5. Bilsborough, A. & Wood, B. A. Cranial morphometry of early hominids: facial region. *Am. J. Phys. Antrhropol.* **76,** 61–86 (1988).
6. Enlow, D. H. & Azuma, M. in *Morphogenesis and Malformations of the Face and Brain* (ed. Langman, J.) 217–230 (Harper and Row, New York, 1975).
7. Enlow, D. H. *Facial Growth* 3rd edn (Saunders, Philadelphia, 1990).
8. Bromage, T. G. The ontogeny of *Pan troglodytes* craniofacial architectural relationships and implications for early hominids. *J. Hum. Evol.* **23,** 235–251 (1992).
9. Duterloo, H. S. & Enlow, D. H. A comparative study of cranial growth in *Homo* and *Macaca*. *Am. J. Anat.* **127,** 357–368 (1970).
10. Bromage, T. G. Ontogeny of the early hominid face. *J. Hum. Evol.* **18,** 751–773 (1989).
11. MacCammon, R. *Human Growth and Development* (C. C. Thomas, Springfield, 1970).
12. Weidenreich, F. The brain and its rôle in the phylogenetic transformation of the human skull. *Trans. Am. Phil. Soc.* **31,** 321–442 (1941).
13. Shea, B. T. On aspects of skull form in African apes and orangutans, with implications for hominid evolution. *Am. J. Phys. Anthropol.* **68,** 329–342 (1985).
14. Ravosa, M. J. Ontogenetic perspective on mechanical and nonmechanical models of primate circumorbital morphology. *Am. J. Phys. Anthropol.* **85,** 95–112 (1991).
15. Trinkaus, E. The Neandertal face: evolutionary and functional perspectives on a recent hominid face. *J. Hum. Evol.* **16,** 429–443 (1987).
16. Spencer, M. A. & Demes, B. Biomechanical analysis of masticatory system configuration in Neanderthals and Inuits. *Am. J. Phys. Anthropol.* **91,** 1–20 (1995).
17. Corruccini, R. M. Metrical reconsideration of the Skhul IV and IX and Border Cave 1 crania in the context of modern human origins. *Am. J. Phys. Anthropol.* **87,** 433–445 (1992).
18. Krings, M. *et al.* Neandertal DNA sequences and the origin of modern humans. *Cell* **90,** 19–30 (1997).
19. Stringer, C. B. & Andrews, P. A. Genetic and fossil evidence for the origin of modern humans. *Science* **239,** 1263–1268 (1988).
20. Schwartz, J. H. & Tattersall, I. Significance of some previously unrecognized apomorphies in the nasal region of *Homo neanderthalensis*. *Proc. Natl Acad. Sci. USA* **93,** 10852–10854 (1996).
21. Howells, W. W. *Skull Shapes and the Map* (Peabody Museum Papers no. 79, Cambridge, 1989).
22. Lieberman, D. E. How and why recent humans grow thin skulls: experimental data on systemic cortical robusticity. *Am. J. Phys. Antropol.* **101,** 217–236 (1996).
23. Ruff, C. B., Trinkaus, E. & Holliday, T. W. Body mass and encephalization in Pleistocene *Homo*. *Nature* **387,** 173–176 (1997).
24. Arensburg, B., Schepartz, L. A., Tillier, A. M., Vandermeersch, B. & Rak, Y. A reappraisal of the anatomical basis for speech in Middle Paleolithic hominids. *Am. J. Phys. Anthropol.* **83,** 137–146 (1990).
25. Stevens, K. N. in *Human Communication: A Unified View* (eds David, E. E. & Denes, P. B.) 51–66 (McGraw Hill, New York, 1972).
26. Fant, G. *Acoustic Theory of Speech Production* (Moulton, The Hague, 1960).
27. Lieberman, P. *The Biology and Evolution of Language* (Harvard Univ. Press, Cambridge, MA, 1984).
28. Aiello, L. & Dean, C. *An Introduction to Human Evolutionary Anatomy* (Academic, London, 1990).
29. White, T. D. & Folkens, P. A. *Human Osteology* (Academic, San Diego, 1991).

Acknowledgements. I thank B. Arensburg, M. Chech, A. W. Crompton, J.-J. Hublin, L. Humphreey, L. Jellema, R. Kruszinski, P. Langaney, B. Latimer, T. Molleson, D. Pilbeam, A. Poole, C. Ross, G. Sawyer, F. Spoor, C. Stringer, I. Tattersall and A. Walker for help and/or permission to obtain radiographs and CT scans; R. McCarthy, K. Mowbray and R. Bernstein for help with collecting data; and L. Aiello, F. A. Jenkins Jr, P. O'Higgins, O. Pearson, D. Pilbeam, G. P. Rightmire, N. Shubin, R. J. Smith, I. Tattersall and B. Wood for comments on the manuscript. This work was supported by Rutgers University.

Correspondence and requests for materials should be addressed to the author (e-mail: danlieb@rci.rutgers.edu).

Gene transfer to the nucleus and the evolution of chloroplasts

William Martin*, Bettina Stoebe†, Vadim Goremykin*, Sabine Hansmann*, Masami Hasegawa‡ & Klaus V. Kowallik†

* *Institut für Genetik, Technische Universität Braunschweig, Spielmannstrasse 7, 38023 Braunschweig, Germany*
† *Botanisches Institut, Heinrich-Heine-Universität Düsseldorf, Universitätsstrasse 1, 40225 Düsseldorf, Germany*
‡ *The Institute of Statistical Mathematics, 4-6-7 Minami-Azabu, Minato-ku, Tokyo 106, Japan*

Photosynthetic eukaryotes, particularly unicellular forms, possess a fossil record that is either wrought with gaps or difficult to interpret, or both. Attempts to reconstruct their evolution have focused on plastid phylogeny, but were limited by the amount and type of phylogenetic information contained within single genes[1–5]. Among the 210 different protein-coding genes contained in the completely sequenced chloroplast genomes from a glaucocystophyte, a rhodophyte, a diatom, a euglenophyte and five land plants, we have now identified the set of 45 common to each and to a cyanobacterial outgroup genome. Phylogenetic inference with an alignment of 11,039 amino-acid positions per genome indicates that this information is sufficient—but just barely so—to

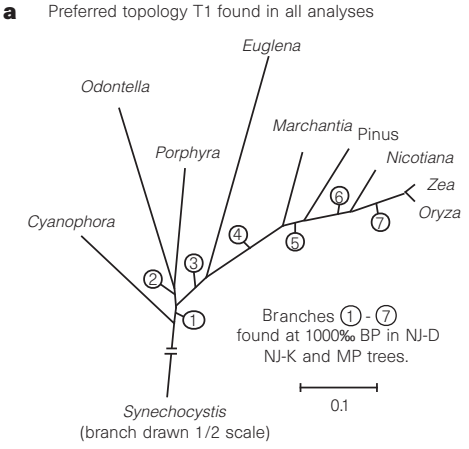

Figure 1 Plastid phylogeny interpreted from chloroplast proteins. **a**, Rooted nine species neighbour-joining (NJ) tree of Dayhoff distances for 11,039 amino-acid positions from 45 orthologous proteins common to these chloroplast genomes and *Synechocystis*. All seven branches of this topology (T1) are found in 1,000/1,000 bootstrap samples in maximum parsimony (PROTPARS of PHYLIP) and NJ analysis using either Kimura or Dayhoff distances. The root of the tree is assumed from the model that all plastids sampled here arose from a common chloroplast ancestor. Branches are numbered 1–7 for convenience (see text). The scale bar indicates Dayhoff distance. **b**, Alternative topologies T2, T3 and T4 detected in protein maximum likelihood[10] analyses using the JTT-F model. Taxon abbreviations are given in Methods; branch 3 is the same as in **a**.